Acta Pharmaceutica Sinica B 2024;14(12):5305−5320

Chinese Pharmaceutical Association
Institute of Materia Medica, Chinese Academy of Medical Sciences

Acta Pharmaceutica Sinica B

www.elsevier.com/locate/apsb
www.sciencedirect.com

ORIGINAL ARTICLE

AKR1C1 interacts with STAT3 to increase intracellular glutathione and confers resistance to oxaliplatin in colorectal cancer

Zhiwen Fu[a,b], Tingting Wu[a,b], Chen Gao[a,b], Lulu Wang[a,b], Yu Zhang[a,b], Chen Shi[a,b,*]

[a]*Department of Pharmacy, Union Hospital, Tongji Medical College, Huazhong University of Science and Technology, Wuhan 430022, China*
[b]*Hubei Province Clinical Research Center for Precision Medicine for Critical Illness, Wuhan 430022, China*

Received 18 March 2024; received in revised form 5 July 2024; accepted 26 July 2024

KEY WORDS

Oxaliplatin resistance;
AKR1C1;
Colorectal cancer;
Alantolactone;
Glutathione;
Combination therapy;
Natural product;
Chemoresistance

Abstract Oxaliplatin (OXA), a platinum-based chemotherapeutic agent, remains a mainstay in first-line treatments for advanced colorectal cancer (CRC). However, the eventual development of OXA resistance represents a significant clinical challenge. In the present study, we demonstrate that the aldo-keto reductase 1C1 (AKR1C1) is overexpressed in CRC cells upon acquisition of OXA resistance, evident in OXA-resistant CRC cell lines. We employed genetic silencing and pharmacological inhibition strategies to establish that suppression of AKR1C1 restores OXA sensitivity. Mechanistically, AKR1C1 interacts with and activates the transcription factor STAT3, which upregulates the glutamate transporter EAAT3, thereby elevating intracellular glutathione levels and conferring OXA resistance. Alantolactone, a potent natural product inhibitor of AKR1C1, effectively reverses this chemoresistance, restricting the growth of OXA-resistant CRC cells both *in vitro* and *in vivo*. Our findings uncover a critical AKR1C1-dependent mechanism behind OXA resistance and propose a promising combinatorial therapeutic strategy to overcome this resistance in CRC.

*Corresponding author.
E-mail address: whxhchen@163.com (Chen Shi).

Peer review under the responsibility of Chinese Pharmaceutical Association and Institute of Materia Medica, Chinese Academy of Medical Sciences.

https://doi.org/10.1016/j.apsb.2024.08.031

1. Introduction

Colorectal cancer (CRC) represents a highly prevalent malignant neoplasm with a major global health burden, surpassing one million new cases diagnosed annually worldwide[1]. Oxaliplatin (OXA), a platinum-based chemotherapy agent, forms a cornerstone of the CRC treatment regimen, commonly administered in combination with 5-fluorouracil and leucovorin (FOLFOX regimen) or capecitabine (CapeOx regimen)[2,3]. While these regimens achieve substantial improvements in the management and outcomes of patients with late-stage colorectal cancer, the development of acquired resistance to OXA presents a significant clinical challenge, often resulting in tumor recurrence, metastasis, and cancer-related mortality[4,5]. Consequently, elucidating the mechanisms underlying OXA resistance represents a critical clinical imperative to develop strategies to prolong the therapeutic efficacy of OXA in the treatment of patients with CRC.

AKR1C1, a member of the aldo-keto reductase family, plays a role in the NADP(H)-dependent reduction of aldehydes and ketones, contributing to the regulation of biosynthesis and intermediary metabolism[6]. Recent evidence has also uncovered the impact of AKR1C1 on cancer initiation, progression, and metastasis[7]. Highly expressed in cancer clinical samples compared with all other normal tissues, AKR1C1 exhibits a promotive influence on cancer cell proliferation, migration, and invasion. Amplification or gain of the AKR1C1 gene occurs with a high degree of frequency across a diverse array of human malignancies and constitutes an adverse prognostic indicator with regard to progression-free survival outcomes in the cancer patient population[8,9]. The aberrant activation of other aldo-keto reductases, such as the AKR1C2, AKR1B10, and AKR1C4, was also shown to promote the growth, migration, and drug resistance of cancer cells[10]. Furthermore, the aldo-keto reductase family exhibits characteristics of stress response genes, demonstrating transcriptional induction in response to drug metabolism, electrophilic and oxidative stress stimuli, osmotic stress, and steroid hormone signaling[11-13]. Owing to their responsiveness to electrophilic and oxidative stress that is induced by chemotherapeutic agents, the expression of these enzymes becomes upregulated upon exposure to such agents, leading to the acquisition of drug resistance[14]. Nonetheless, while prior studies have provided evidence implicating AKR1C1 in cancer cell growth and progression, its specific role in mediating the chemotherapeutic response and OXA resistance in CRC remains unexplored, with the underlying mechanisms yet to be elucidated. In the present study, we investigated the direct contribution of AKR1C1 and its associated signaling pathway to the development and maintenance of OXA resistance in CRC, as well as the potential for targeting this pathway to overcome OXA resistance.

2. Materials and methods

2.1. Cell lines culture

The human colorectal cancer cell lines HCT116, SW480, and HT-29 were obtained from the Cell Bank of Type Culture Collection of the Chinese Academy of Sciences (Shanghai, China). The HCT116 and its OXA-resistant cell line were cultured in the Dulbecco's modified Eagle's medium (Gibco) supplemented with 10% fetal bovine serum (Gibco) and 1% penicillin−streptomycin (Gibco). The cells were maintained in a humidified incubator at 37 °C with 5% CO_2.

2.2. Cell viability assay

The cell viability for both the cell proliferation and cytotoxicity assay was measured using the Cell Counting Kit-8 (CCK-8, Beyotime, China) according to the manufacturer's instructions. Briefly, after the completion of drug treatment, 10 μL of the CCK-8 solution was added to each well of the plate and the plate was incubated for 4 h in the cell incubator. The absorbance was then recorded at 450 nm using a microplate reader (PerkinElmer). The cell viability curves were plotted by GraphPad Prism 9.0.

2.3. Synergistic effect analysis

In order to determine the synergistic effect of drug combinations, we employed the online SiCoDEA App (Single and Combined Drug Effect Analysis) for analyzing the effect of individual drugs and their combinations, which is available at: https://sicodea.shinyapps.io/shiny/. This app utilizes both the response surface model and the zero interaction potency (ZIP) calculation method to determine the "inhibition index". When interpreting these results, ZIP synergy scores greater than 0 suggest a synergistic effect, while scores greater than 10 suggest a strong synergistic effect. In addition to these calculations, we utilized heat maps of drug combination responses to assess the clinical applicability of these pairings. These heatmaps provided a visual demonstration of the drug synergy scores, allowing us to identify the most effective drug combinations for the treatment of colorectal cancer.

2.4. Colony formation assay

After the treatment with vehicle or indicated drugs, cells were seeded into 6-well plates with a single-cell suspension at a density of 200 cells per well and allowed to grow for 2−3 weeks until large colonies were visible. Crystal violet (0.05%, Sigma−Aldrich) was used to stain the colonies then the images were captured by a light-filed microscope and the number of clearly visible colonies was counted.

2.5. Immunofluorescence

The cells were cultured in confocal dishes and fixed with 4% paraformaldehyde in PBS (Thermo Scientific). After permeabilization with 0.2% Triton X-100 (Sigma−Aldrich) for 10 min followed by three times PBS washing, the cells were blocked with 2% BSA for 30 min. The cells were then incubated with anti-AKR1C1 and STAT3 antibodies (1:200, Abcam) overnight at 4 °C. The cells were washed and incubated with fluorescent secondary antibodies for 1 h. The nuclei were counterstained with DAPI (4′,6-diamidino-2-phenylindole, Invitrogen). After washing with PBS, the cells were then observed using a fluorescence microscope (Zeiss).

2.6. Immunoblot analysis

Cells were treated with various concentrations of drugs and harvested for immunoblotting analysis as previously reported. Briefly, the RIPA lysis and extraction buffer (Thermo Scientific) with a protease inhibitor cocktail (Roche) was used to homogenize both cells and tumor tissues. After the protein concentration determination and denaturation, the lysate samples were separated by electrophoresis using the 6%−15% polyacrylamide gel followed by transferring to a polyvinylidene difluoride membrane. Then the

membrane was incubated with desired primary antibodies after blocking with 5% bovine serum albumin in TBST solution (Tris-buffered saline with 0.1% Tween-20). After three times TBST washing, the membrane was incubated with the homologous horseradish peroxidase-linked secondary antibody. The chemiluminescence was captured and recorded in digital images or photographic films.

2.7. RNA-seq analysis

Triplicate RNA samples from parental HCT116 cell lines ($n = 3$) and OXA-resistant HCT116 cell lines ($n = 3$) were extracted using a total RNA extraction kit (Qiagen) and subjected to RNA sequencing at Wuhan Frasergen Co., Ltd. The raw data was filtered and FastQC software (version 0.12.0) was used to remove reads with low quality and joint sequences from the sequencing results. The rRNA contamination rate of each sample was determined by Bowtie2 software (version 2.5.1) through the comparison between clean data and the eukaryotic rRNA database. Then, the clean data was compared with reference genomes using HISAT2 software (version 2.2.1) to determine the distribution of reads on the reference genome. To identify the expression of genes and isoforms, StringTie software (version 2.2.0) was used to predict transcripts of all samples, and then RSEM software (version 1.3.3) was used to call comparison results of Bowtie2 for statistics, and calculated the number of reads of each sample. In addition, FPKM (fragments per kilobase per million bases) transformations were performed, and paired-end reads from the same fragment were counted as one fragment. The differentially expressed genes (DEGs) were determined from the expected_count using R software with the DESeq2 package. The filter thresholds were set as FDR (false discovery rate) <0.05, log FC (fold change (condition 2/condition 1) for a gene) >1 or log FC<-1 and p-adj<0.01. Pathway analysis and Gene Ontology (GO) analysis were applied to determine the functions of those differentially expressed mRNAs by GO (www.geneontology.gov) and the KEGG (Kyoto Encyclopedia of Genes and Genomes) pathway database (http://www.genome.jp/kegg/pathway.html). The FDR<0.05 was considered to be significant.

2.8. RNA extraction and qPCR analysis

The RNA samples were extracted using a total RNA extraction kit (Qiagen) and concentrations were determined by NanoDrop One (Thermo Scientific). And the RNA was reverse transcribed to cDNA using the RT2 Easy First Strand Kit (Qiagen) according to the instructions from the manufacturer followed by the PCR assay. The real-time data were recorded and analyzed using the LightCycler 480 Real-Time PCR System (Roche) with the QuantiTect SYBR Green PCR Kits (Qiagen).

2.9. Measurement of reactive oxygen species levels

Cells were seeded at a density of 2×10^5 cells per well in 6-well tissue culture plates and incubated overnight at 37 °C to allow for adherence and recovery. Subsequently, the cells were incubated with 2′,7′-dichlorofluorescin diacetate (DCFDA, Sigma−Aldrich; 25 μmol/L) in Hanks' Balanced Salt Solution (Thermo Scientific) at 37 °C for 45 min to facilitate the intracellular accumulation and deacetylation of the probe. Following incubation, the cells were washed with PBS to remove the excess staining probe, and either left untreated (vehicle control) or treated with the indicated agents. Fluorescence emission, indicative of intracellular reactive oxygen species levels, was quantified at an excitation/emission wavelength of 485/535 nm using FACS flow cytometry (BD Biosciences).

2.10. Intracellular GSH and GSSG levels

To measure reduced glutathione levels in tumor tissues and cell lysates, we utilized the Reduced GSH Assay Kit (Sigma−Aldrich) according to the manufacturer's protocol. Briefly, tumor tissue or cell suspensions were divided into two equal sets, one of which was homogenized with 5% sulfosalicylic acid to measure GSH levels, the absorbance was measured at 450 nm every 5 min in a kinetics mode. To determine glutathione disulfide (GSSG) levels, we used the GSH/GSSG assay kit following the manufacturer's instructions. We added a scavenger to the cell lysate to remove any existing GSH and then measured the absorbance of each sample at 412 nm.

2.11. Gene knockdown siRNA transfections

Following an overnight adherence period, cells were seeded on six-well plates with a confluence level moderated between 40% and 60%. Subsequently, transfection was conducted using Lipofectamine 3000 (Invitrogen) following the manufacturer's guidelines with 20 nmol/L of siRNA duplexes (GenePharma). Gene knockdown was assessed through Western blot and RT-qPCR analysis after 48 h of transfection. Mock siRNA duplexes were administered to cells as a control. Further details regarding the target sequences for siRNAs can be found in Supporting Information Table S1.

2.12. Establishment of AKR1C1-overexpressed stable cell lines

To generate lentiviruses, lentiviral envelop plasmid pMD2.G and packaging plasmid psPAX2 (Addgene) were transfected into 293FT packaging cells (Thermo Scientific). The negative control was represented by an empty vector. After a transfection period of 48 h, lentiviral supernatants were collected. Cells were subsequently transduced with lentiviruses containing polybrene and selected using puromycin (1 μg/mL). Western blot analysis was performed to assess the expression of AKR1C1 after selection.

2.13. Co-immunoprecipitation

After transfection with FLAG-AKR1C1 and HA-STAT3 for 48 h, the cells were lysed in NP-40 lysis buffer (50 mmol/L Tris-HCl, pH 7.4, 150 mmol/L NaCl, 1% NP-40) supplemented with a protease inhibitor cocktail (Roche). The cell lysates were then incubated with the indicated magnetic tag-beads (Sigma−Aldrich) at 4 °C overnight followed five times lysis buffer washing. The enriched proteins were eluted through boiling in the SDS loading buffer for 5 min and subjected to immunoblotting analysis with indicated antibodies.

2.14. Tumor xenograft models

Six-week-old BALB/c nude mice used in this study were purchased from Beijing Charles River Laboratories (Beijing, China) and housed in a specific pathogen-free environment in the animal facility. All animals were fed and experimented in accordance with the requirements of the ethical guidelines for laboratory animals of

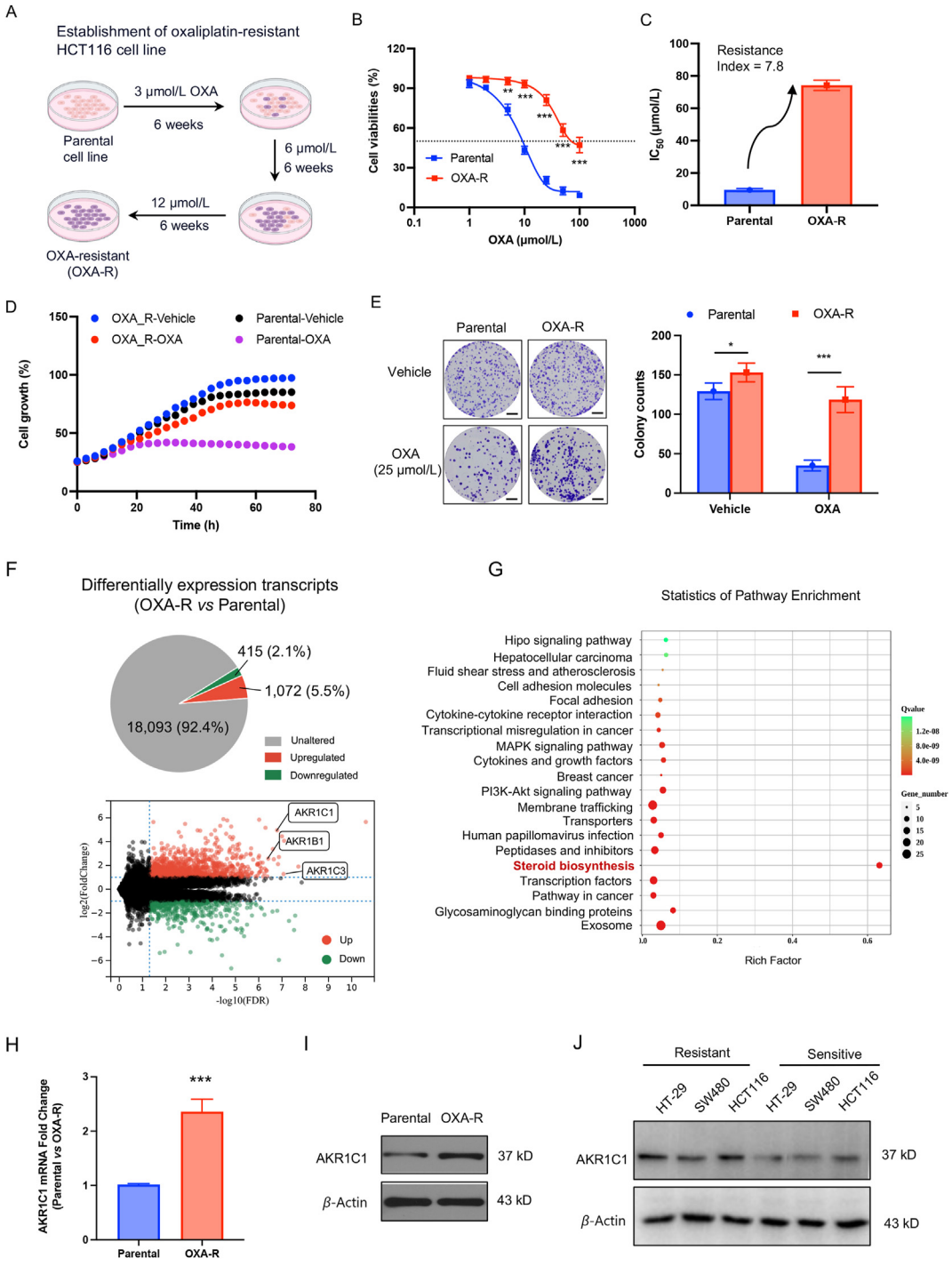

Figure 1 Identification of AKR1C1 as a target for oxaliplatin-resistant (OXA-R) colorectal cancer. (A) Experimental scheme to establish OXA-resistant colorectal HCT116 cancer cell lines. (B) The parental and OXA-resistant HCT116 cell lines were exposed to different concentrations of OXA for 72 h and the cell viability was determined by the CCK-8 assay. Data are mean ± SD ($n = 6$). $^{**}P < 0.01$ and $^{***}P < 0.001$ *versus* matched parental cells. (C) IC_{50} (μmol/L, 72 h) values were calculated from survival curves, and the resistance index (RI) was calculated by dividing the IC_{50} for OXA-R cells by that of parental cells. (D) Cell growth analysis of HCT116 and HCT116/OXA-R cells. Cells were treated with vehicle or 25 μmol/L OXA for 72 h. (E) A clonogenic assay was carried out to assess the effect of vehicle and OXA on the colony formation capability of HCT116 and HCT116/OXA-R cells. The histograms represent the number of colonies. Data are mean ± SD ($n = 4$). $^{*}P < 0.05$, $^{***}P < 0.001$, compared with control. Scale bar, 5 mm. (F) The pie chart and volcano plot illustrate the differentially expressed genes between parental and OXA-R HCT116 cells in the RNA-seq data set. Significantly differentially expressed transcripts matching the threshold (>2-fold) and the statistical analysis standard adjusted P value (FDR) < 0.05 were selected. The up-regulated genes are shown in red and the down-regulated genes in green. (G) KEGG pathway analysis of the regulated targets in parental cell *versus* OXA-R cells transcriptome. (H, I) AKR1C1 overexpression in HCT116/OXA-R cells was assessed using reverse transcription-quantitative polymerase chain reaction analysis (H, $^{***}P < 0.001$) and Western blotting (I). (J) Expression of AKR1C1 was increased in OXA-resistant three colorectal cancer cell lines compared to those of matched parental cancer cell lines.

Huazhong University of Science and Technology. Our study was approved ([2023] IACUC Number: 30921) by the Institutional Animal Care and Use Committee of Tongji Medical College, Huazhong University of Science and Technology. The xenograft model was used in this study. Briefly, four million cancer cells in 100 μL PBS were subcutaneously injected into the right flank region of the mice. When the average tumor volume reached 100 mm^3, the tumor-bearing mice were randomly divided into groups and administered with either the vehicle or different drugs as indicated. The mice were closely monitored daily, and the changes in body weight and tumor size were recorded every 3−4 days. Tumor volumes were measured with calipers and calculated using Eq. (1):

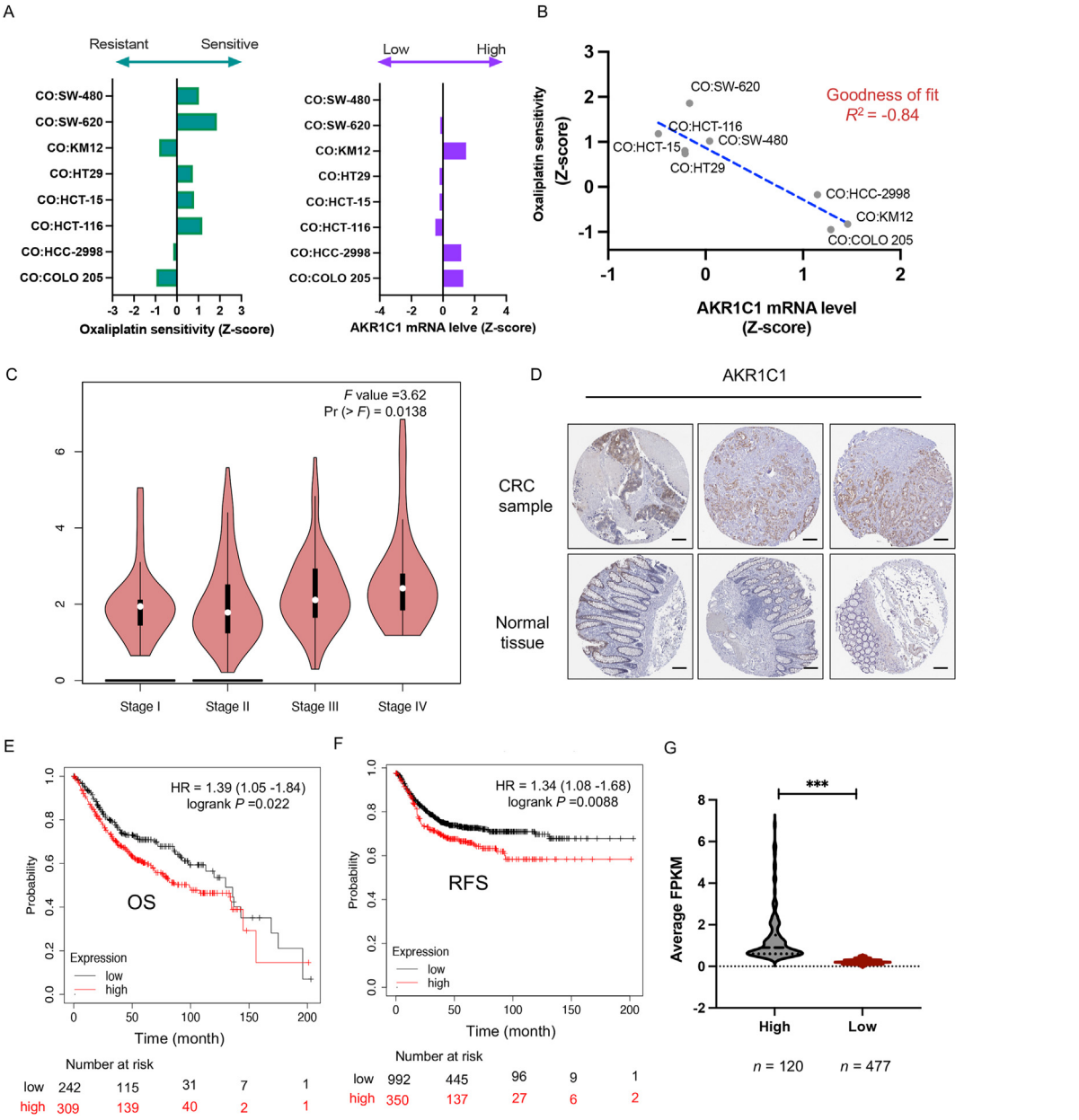

Figure 2 AKR1C1 is associated with oxaliplatin (OXA) sensitivity and poor prognostics in colorectal cancer. (A) AKR1C1 expression is negatively correlated with OXA therapeutic response in colorectal cancer cell lines from NCI-60 cancer cell lines. The sensitivity of representative colorectal cancer cell lines to OXA is represented by the z-score, with cells categorized as sensitive (0−3) or resistant (0 to −3). And AKR1C1 expression in representative colorectal cancer cell lines is represented by the z-score, with expression categorized as high (0−4) or low (0 to −4). (B) AKR1C1 mRNA expression is inversely correlated with the sensitivity of colorectal cancer cell lines to OXA treatment ($R^2 = -0.84$). (C) The expression of *AKR1C1* mRNA transcripts in patients with normal colon and colorectal adenocarcinoma by stage. (D) AKR1C1 expression levels in the colorectal cancer tissues were higher than that of matched adjacent non-cancerous tissues. Representative IHC images are presented. Scale bar, 150 μm. (E, F) The overall survival (OS) and relapse-free survival (RFS) curves for colorectal cancer patients with different expression levels of AKR1C1 according to the Kaplan−Meier plotter database. *P* values and hazard ratios (HRs) are shown. (G) The *AKR1C1* mRNA level in the high-expression ($n = 120$) and low-expression ($n = 477$) groups. RNA-seq data is reported as average FPKM (number of Fragments Per Kilobase of exon per Million reads), generated by The Cancer Genome Atlas (TCGA). ***$P < 0.001$.

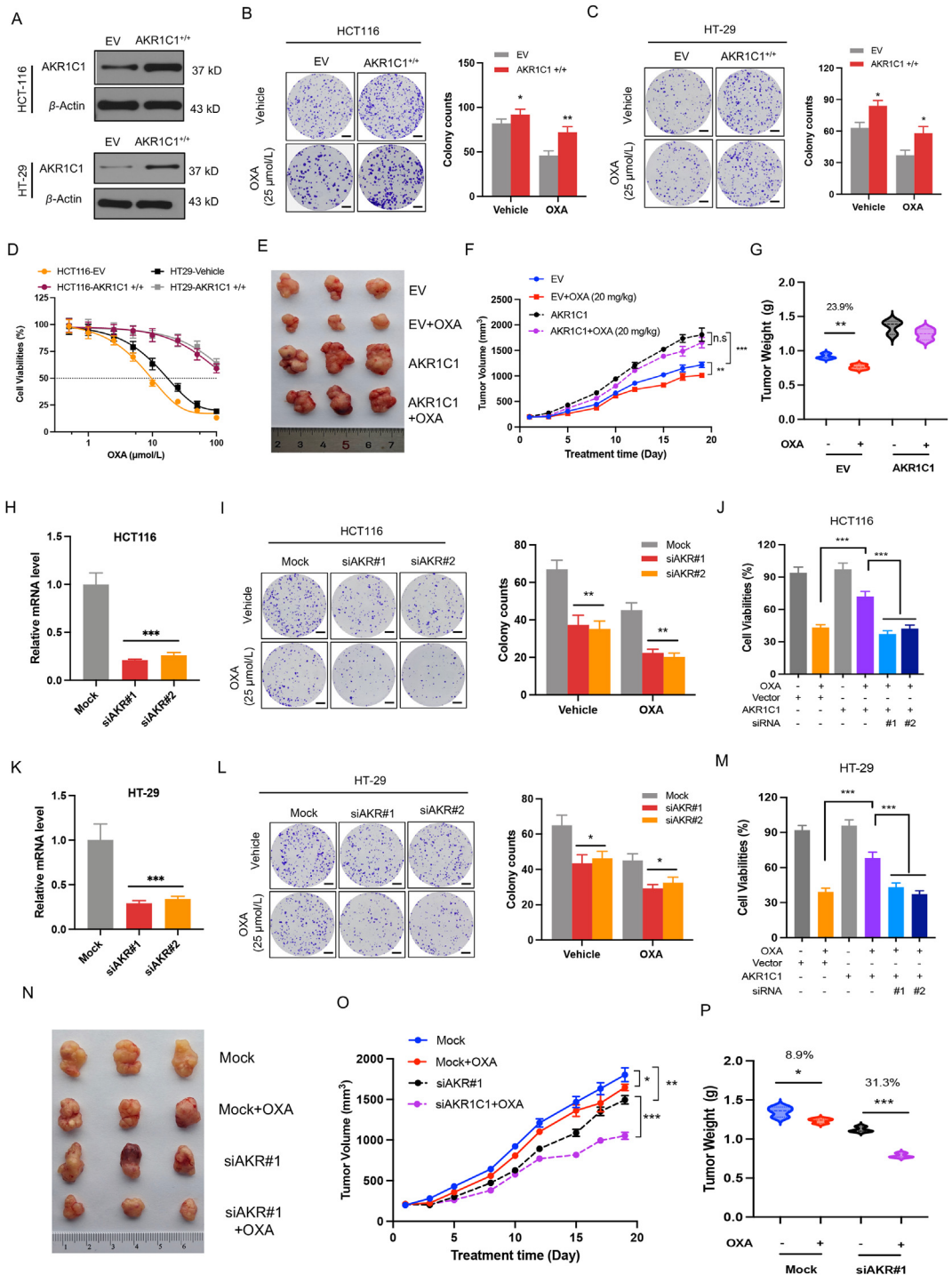

Figure 3 AKR1C1 confers resistance to oxaliplatin (OXA) in the colorectal cancer cells. (A) Western blot analysis on HCT116 and HT-29 parental cells transduced with the empty vector (EV) and AKR1C1 expressing lentivirus (*AKR1C1*$^{+/+}$) cells to determine AKR1C1 expression. (B, C) Colony formation assays in HCT116 (B) and HT-29 (C) colon cancer cells stably expressing empty vector (EV) or AKR1C1. Representative images and quantification (mean ± SD, $n = 3$) are shown. *$P < 0.05$, **$P < 0.01$. Scale bar, 5 mm. (D) Dose−response curves of EV and AKR1C1 overexpressing cells treated with increasing OXA doses for 72 h (mean ± SD, $n = 4$). (E) Representative images of explanted tumors are presented. Scale bar, 1 cm. (F) Tumor growth curves of HCT116-EV and HCT116-AKR1C1 xenografts in nude mice treated with OXA (mean ± SD, $n = 3$). ns, no significance, **$P < 0.01$, ***$P < 0.001$ (G) Tumor weight measurements at the endpoint of the xenograft study (mean ± SD, $n = 3$). **$P < 0.01$. (H) The expression of AKR1C1 in HCT116 cells transfected with Mock and two siAKR1C1 agents was evaluated by qRT-PCR. ***$P < 0.001$. (I) Colony formation assays in HCT116 cells were transiently transfected with non-targeting (Mock) or AKR-targeting siRNAs (siAKR#1, siAKR#2) and treated with 25 μmol/L OXA. Representative images and quantification (mean ± SD, $n = 3$) are shown. *$P < 0.05$, **$P < 0.01$ *versus* mock. Scale bar, 5 mm. (J) Effects of AKR1C1 expression on OXA sensitivity in HCT116 cells. The cells transiently transfected with AKR-targeting siRNAs (siAKR#1, siAKR#2) or AKR1C1 and then the cell viability was determined by the

$$V = 0.52 \times W^2 \times L \quad (1)$$

where W and L represent the smallest and largest superficial diameters, respectively. At the end of the study, all mice were humanely euthanized, and the tumor samples were collected and weighed.

2.15. Immunohistochemistry analysis

The tumor tissue was fixed in 4% formalin and embedded in paraffin before being sliced into 3 μm thick sections. The sections were deparaffinized using EZ solution (Roche) and subjected to antigen retrieval, followed by endogenous peroxidase (3% H_2O_2) blocking. The primary antibodies, including anti-AKR1C1 (Cell Signaling Technology, 1:200), anti-EAAT3 (Cell Signaling Technology, 1:200), and anti-STAT3 (Abcam, 1:200), were applied and incubated at room temperature for 1 h. Then, secondary antibodies were added and incubated for 30 min at room temperature. Subsequently, the DAB kit (Roche) was applied sequentially to stain the slides. After nuclear counterstaining with hematoxylin and mounting coverslips with mounting medium, the slides were examined under a light-field microscope (Zeiss Axiovert 200).

2.16. Statistical analysis

The mean values along with their corresponding standard deviations (SD) were obtained from at least three independent experiments in this study and expressed as mean ± SD. Statistical analysis was carried out using the Student's *t*-test for comparison of two groups or using the Analysis of Variance (ANOVA) for more than two groups. Statistical significance was considered when $P < 0.05$.

2.17. Data access

The raw data of RNA-seq was subject to deposit in Gene Expression Omnibus (No. GSE235026).

3. Results

3.1. Identification of AKR1C1 as a target for OXA-resistant colorectal cancer

To investigate the mechanisms underlying resistance to OXA and explore potential therapeutic strategies, we employed a stepwise dose-escalation method (Fig. 1A) to establish OXA-resistant cell lines. Subsequently, we performed CCK-8 assays to assess OXA sensitivity in both parental and drug-resistant cells. Our results reveal a significant decrease in OXA sensitivity in the resistant cells, as evidenced by a higher IC_{50} value (Fig. 1B) with a resistance index of 7.8 (Fig. 1C). Compared to the parental cells, the established OXA-resistant cells proliferate more actively and are less sensitive to the OXA treatment (Fig. 1D). Furthermore, colony formation assays were conducted to evaluate cell sensitivity to OXA treatment, demonstrating a higher number of colonies in the resistant cells following exposure to 25 μmol/L OXA compared to the parental cells (Fig. 1E, $P < 0.001$).

To gain insight into the critical factors associated with OXA resistance in colorectal cancer, we conducted RNA-seq analysis of the HCT116 cell lines, comprising both parental and OXA-resistant (OXA-R) cells. Among the total 19,580 transcripts detected, 1487 transcripts exhibited differential expression between OXA-R and parental cells (1072 up-regulated and 415 down-regulated transcripts) (accession number GEO: GSE235026) (Fig. 1F). Subsequent KEGG pathway analysis identified the steroid biosynthesis pathway as the most up-regulated pathway (Fig. 1G). Specifically, the aldo-keto reductase superfamily, encompassing AKR1C1, AKR1B1, and AKR1C3, known for their involvement in redox transformations associated with steroid biosynthesis, displayed significantly higher expression levels in the OXA-R cells compared to parental cells, consistent with the KEGG pathway analysis. Quantitative real-time PCR confirmed that among the three aldo-keto reductase superfamily genes, *AKR1C1* exhibited the highest expression in OXA-R cells, with levels more than two-fold higher than those in parental cells (Fig. 1H and Supporting Information Fig. S1). The upregulation of AKR1C1 at the protein level was further validated through immunoblotting analysis (Fig. 1I). Moreover, the overexpression of AKR1C1 in the resistant colorectal cancer cells was confirmed in the HT-29 and SW480 cells (Fig. 1J). Collectively, these findings highlight AKR1C1 as a specific marker for OXA resistance and propose it as a promising therapeutic target for overcoming OXA resistance in colorectal cancer.

3.2. AKR1C1 is associated with OXA sensitivity and poor prognostics in colorectal cancer

In light of the above-obtained results, we next aimed to investigate the potential correlation between AKR1C1 expression levels and the therapeutic response to OXA. Utilizing the CellMiner tool (Supporting Information Tables S2 and S3), we examined the OXA sensitivity of representative colorectal cancer cell lines from the NCI-60 cancer cell lines in relation to AKR1C1 expression (Fig. 2A). The quantitative analysis revealed a significant negative correlation, as indicated by the simple linear regression (Good of fitness, $R^2 = -0.84$) (Fig. 2B). These findings suggest that higher AKR1C1 expression is associated with a lower sensitivity of colorectal cancer cells to OXA treatment.

To further explore the role of AKR1C1 in colorectal cancer progression, we analyzed AKR1C1 transcript levels across different stages of colorectal cancer. While a trend was observed, indicating a positive correlation between AKR1C1 expression and

CCK-8 assay (mean ± SD, $n = 3$, $^{***}P < 0.001$). (K) The expression of AKR1C1 in HT-29 cells transfected with Mock and two siAKR1C1 agents was evaluated by qRT-PCR. $^{***}P < 0.001$. (L) Colony formation assays in HT-29 cells were transiently transfected with non-targeting (Mock) or AKR-targeting siRNAs (siAKR#1, siAKR#2) and treated with 25 μmol/L OXA. Representative images and quantification of colony formation are shown (mean ± SD, $n = 3$). $^{*}P < 0.05$, $^{**}P < 0.01$ *versus* mock. Scale bar, 5 mm. (M) Effects of AKR1C1 expression on HT-29 cells. The cells transiently transfected with AKR-targeting siRNAs (siAKR#1, siAKR#2) or AKR1C1, and the cell viability was determined by the CCK-8 assay (mean ± SD, $n = 3$, $^{***}P < 0.001$). (N) Representative images of explanted tumors are presented (Scale bar, 1 cm) and tumor growth curves (O) from a xenograft study assessing the impact of siAKR#1 on OXA response (20 mg/kg). Data are shown as mean ± SD. $^{*}P < 0.05$, $^{**}P < 0.01$, and $^{***}P < 0.001$. (P) Quantification of tumor weights at the endpoint of the siAKR#1 xenograft study ($n = 3$). Data are shown as mean ± SD. $^{*}P < 0.05$, and $^{***}P < 0.001$.

colorectal cancer staging, statistical significance was achieved in stage IV (metastatic) colorectal cancer (Fig. 2C). Moreover, the higher expression of AKR1C1 was demonstrated in the CRC samples compared to the matched adjacent non-cancerous tissues (Fig. 2D). To corroborate these findings, we conducted an additional analysis using the Kaplan−Meier plotter database, which demonstrated that colorectal cancer patients with higher AKR1C1 expression exhibited lower probabilities of overall survival (OS, $P = 0.022$) and relapse-free survival (RFS, $P = 0.0088$) (Fig. 2E and F). The survival results were consistent with findings in the Human Protein Atlas database (+https://www.proteinatlas.org/ENSG00000187134-AKR1C1/pathology/colorectal+cancer) and the AKR1C1 expression level in the high-expression and low-expression groups were demonstrated in Fig. 2G. These results provide compelling evidence that elevated AKR1C1 expression is not only associated with a lower sensitivity of colorectal cancer cells to OXA treatment but also serves as an unfavorable prognostic factor for CRC patients.

3.3. *AKR1C1 confers resistance to OXA in the colorectal cancer cells*

Considering the association between AKR1C1 expression, OXA sensitivity, and prognosis, we sought to investigate the impact of AKR1C1 modulation on chemotherapy sensitivity in colorectal cancer cells. To assess this, we conducted a colony formation assay exposed to 25 μmol/L OXA using HCT116 cells and HT-29 cells overexpressing AKR1C1 and empty vector (EV), respectively (Fig. 3A). As shown in Fig. 3B and C, the results demonstrated that AKR1C1 overexpression in both HCT116 cells and HT-29 cells led to significantly higher number of colonies compared to EV-control cells. Consistent findings were observed in cellular viability assays, where increased AKR1C1 expression in HCT116 cells and HT-29 cells resulted in a shift in sensitivity to OXA compared to the control cells (Fig. 3D). To further examine the effects of AKR1C1 overexpression on tumor growth *in vivo*, we utilized xenograft models derived from EV-control and AKR1C1-overexpressing cells in BALB/c *nu/nu* mice. The EV-control cell-derived xenograft (CDX) subcutaneous flank tumors demonstrated a favorable response to OXA treatment, as evidenced by reduced tumor volumes following drug administration (Fig. 3E). In contrast, the AKR1C1-overexpressing cell-derived CDX tumors displayed significantly reduced sensitivity to OXA treatment, as indicated by notable differences in tumor volume and tumor weight (Fig. 3F and G).

To investigate whether AKR1C1 knockdown could enhance the sensitivity of colorectal cancer cells to OXA, we established Mock and siAKR1C1 HCT116 cells for *in vitro* and *in vivo* examinations (Fig. 3H). Notably, the knockdown of AKR1C1 resulted in a significant decrease in colony counts upon treatment with 25 μmol/L of OXA (Fig. 3I). Furthermore, siAKR1C1 HCT116 cells exhibited increased sensitivity to OXA when treated with varying concentrations of the drug (Fig. 3J). Similar suppression of cell proliferation and increased sensitivity to OXA were confirmed in the HT-29 cells with the silence of AKR1C1 (Fig. 3K−M). Consistent outcomes were observed in the mice xenograft models, as the mean tumor volume of the control group was significantly larger than that of the siAKR1C1 group ($P < 0.01$, Fig. 3N and O), suggesting AKR1C1 knockdown significantly increased sensitivity to OXA treatment. These results were further supported by the mean tumor weight at the experimental endpoint, confirming that AKR1C1 knockdown inhibited tumor proliferation and improved sensitivity to OXA *in vivo* (Fig. 3P). Collectively, these findings suggest that AKR1C1 expression in colorectal cancer contributes to OXA resistance, while suppression of AKR1C1 through molecular knockdown can enhance the sensitivity of colorectal cancer cells to OXA.

3.4. *AKR1C1 increases intracellular glutathione levels to promote OXA resistance in colorectal cancer cells*

Cellular redox homeostasis is a fundamental requirement for cancer cell survival and growth, and a primary mechanism contributing to OXA resistance in colorectal cancer cells[15]. To investigate whether OXA resistance alters cellular redox homeostasis, we employed a commercial Fluorometric Detection Assay Kit to determine the intracellular levels of reduced glutathione (GSH) and GSSG (oxidized glutathione). Our findings demonstrated significantly higher levels of both GSH and GSSG in OXA-resistant HCT116 cancer cells compared to parental cells ($P < 0.001$) (Fig. 4A). Furthermore, the findings demonstrated a preferential conversion of GSH to its reduced form relative to its oxidized disulfide (GSSG) in the chemoresistant cell lines, resulting in an elevated ratio of reduced GSH to oxidized GSSG. Since intracellular GSH serves as the primary antioxidant involved in maintaining cellular redox homeostasis, the corresponding ROS level in the OXA-resistant cells demonstrated a significant decrease ($P < 0.001$, Fig. 4B). We further observed that the depletion of cystine from the culture medium resulted in a selective decrease in intracellular glutathione levels (Fig. 4C) in the chemoresistant HCT116 cell lines and cystine deprivation could also resensitize the resistant cells to OXA treatment (Fig. 4D). In contrast, upregulation of glutathione biosynthesis conferred OXA resistance in chemosensitive cell lines. As shown in Fig. 4E and F, the supplementation of the culture medium with *N*-acetylcysteine (NAC), a cell-permeable cysteine precursor, and glutathione prodrug, attenuated the sensitivity of parental cell lines to OXA and diminished the accumulation of intracellular reactive oxygen species in HCT116 (Fig. 4E) and HT-29 cells (Fig. 4F).

Knockdown of AKR1C1 abrogated the enhanced intracellular content of glutathione and GSSG in HCT116 cells and HT-29 cells, as well as the ratio of GSH/GSSG (Fig. 4G and H). On the contrary, ectopic expression of AKR1C1 in these two cell lines markedly increased the ratio of GSH/GSSG (Fig. 4I). Concordant with these findings, cells engineered to ectopically overexpress AKR1B1 exhibited diminished levels of reactive oxygen species, an effect that was abrogated upon AKR1B1 knockdown (Fig. 4J and K). To further validate the role of AKR1C1 in glutathione-dependent chemoresistance, we examined whether the chemosensitizing effects of AKR1C1 suppression in resistant cells could be rescued by augmenting the glutathione biosynthetic pathway. Cell viability assays demonstrated that AKR1C1 inhibition substantially resensitized chemoresistant cell lines to OXA, an effect that was attenuated by supplementation with the glutathione precursor NAC (Fig. 4L). These data indicate that AKR1C1 confers OXA resistance in the colorectal cancer cells in a GSH-dependent manner.

3.5. *AKR1C1 up-regulates EAAT3 by activating STAT3 to increase intracellular GSH and confers OXA resistance*

Since the excitatory amino acid transporter (EAAT) family plays an important role in intracellular glutathione, we next investigated

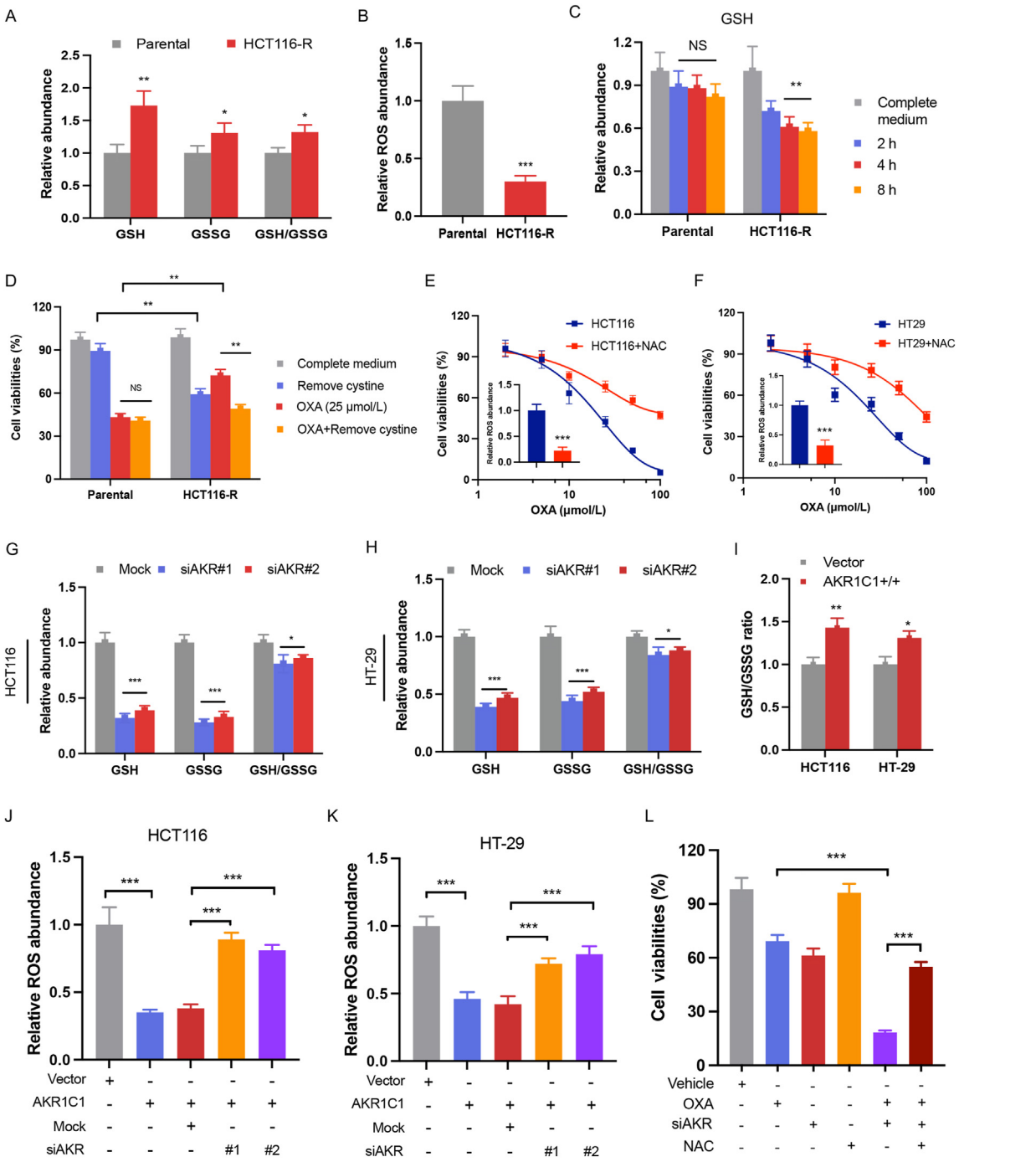

Figure 4 AKR1C1 increases intracellular glutathione levels to promote oxaliplatin (OXA) resistance in colorectal cancer cells. (A) Quantification of reduced glutathione (GSH), oxidized glutathione (GSSG), and their redox ratio in parental and HCT116-R colon cancer cells under different conditions (GSH, GSSG, GSH/GSSG). Data are mean ± SD ($n = 3$). $^{*}P < 0.05$, $^{**}P < 0.01$. (B) Relative fold change in intracellular ROS level in parental and HCT116-R cells. Data are mean ± SD ($n = 3$). $^{***}P < 0.001$. (C) Kinetics of GSH depletion in parental and HCT116-R cells exposed to complete medium or medium lacking cysteine for the indicated time points. Data are mean ± SD ($n = 3$). NS, no significance. $^{**}P < 0.01$. (D) Effect of modulating cysteine availability on cell viability in parental and HCT116-R cells. Cells were treated with the indicated conditions for 48 h before evaluation. Data are mean ± SD ($n = 3$). $^{**}P < 0.01$. (E, F) Dose−response curves for cell viability upon treatment with the glutathione precursor *N*-acetylcysteine (NAC) in parental and HCT116-R cells (E), and HT29 cells (F). Intracellular ROS level was determined as the indicator of NAC administration. Data are mean ± SD ($n = 3$). $^{***}P < 0.001$. (G, H) Effect of knockdown of AKR1C1 by siRNAs (siAKR#1, siAKR#2) on the GSH, GSSG, and GSH/GSSG ratio in HCT116 (G) and HT-29 (H) cells. Cells were transfected with 10 nmol/L AKR1C1 siRNAs or mock siRNA control for 48 h. Data are mean ± SD ($n = 3$). $^{*}P < 0.05$, $^{**}P < 0.01$, $^{***}P < 0.001$ *versus* mock group. (I) The ratio of GSH/GSSG in HCT116 and HT-29 cells stably expressing AKR1C1 was determined. Data are mean ± SD ($n = 3$). $^{*}P < 0.05$, $^{**}P < 0.01$. (J, K) Relative ROS abundance upon treatment with the indicated combinations in HCT116 (J) and HT-29 (K) cells. The cells transiently transfected with AKR-targeting siRNAs (siAKR#1, siAKR#2) or AKR1C1, and the ROS was determined by the flow cytometry (mean ± SD, $n = 3$, $^{***}P < 0.001$). (L) Cell viability upon treatment with the indicated combinations in OXA-resistant HCT116 cells. Data are mean ± SD, $n = 3$. $^{***}P < 0.001$.

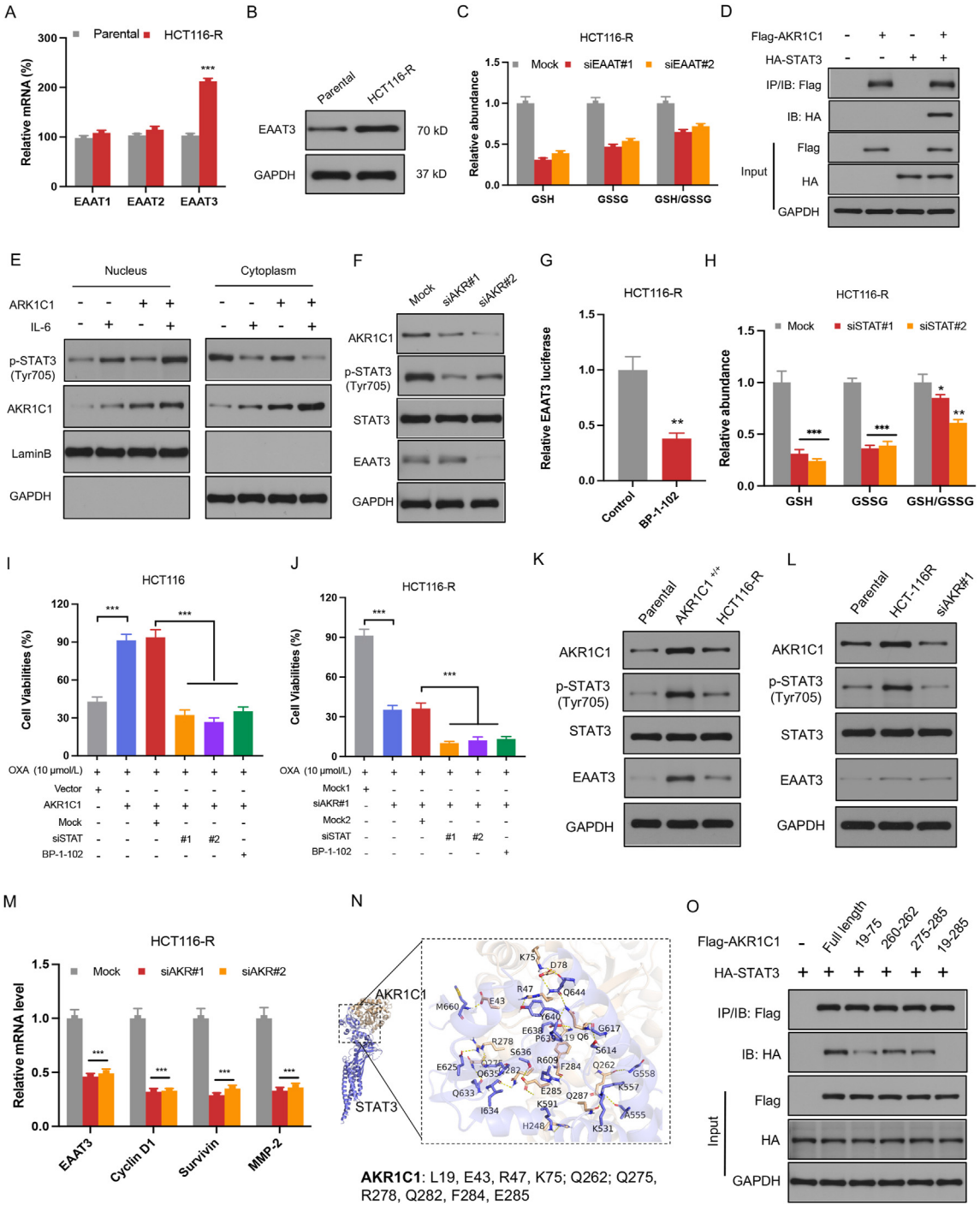

Figure 5 AKR1C1 up-regulates EAAT3 by activating STAT3 to increase intracellular GSH and confers oxaliplatin (OXA) resistance. (A) Quantitative RT-PCR analysis of EAAT1, EAAT2, and EAAT3 mRNA levels in parental and HCT116-R colorectal cancer cells. Data are mean ± SD ($n = 3$). ***$P < 0.001$ *versus* parental cells. (B) Western blot analysis of EAAT3 protein expression in parental and HCT116-R cells. GAPDH served as a loading control. (C) Relative abundances of GSH, GSSG, and the GSH/GSSG ratio in mock-treated cells or cells transfected with siRNAs targeting EAAT3 (siEAAT#1 or siEAAT#2). Data are mean ± SD ($n = 3$). (D) Co-immunoprecipitation of Flag-AKR1C1 and HA-STAT3 in HCT116-R cells assessed by Western blotting. IP, immunoprecipitation; IB, immunoblotting. (E) AKR1C1 increases STAT3 nuclear translocation. HCT116 cells stably expressing AKR1C1 were treated with IL-6 for 30 min after starving overnight. Subcellular localization of AKR1C1 and phosphor-STAT3 (Tyr705) was detected by Western blotting. Lamin B served as a nuclear marker while GAPDH served as a cytoplasmic marker of HCT116-R cells. (F) Western blot analysis of AKR1C1, phosphor-STAT3 (Tyr705), total STAT3, and EAAT3 in mock and HCT116-R cells. (G) Effect of STAT3 inhibition (2 μmol/L of BP-1-102, 16 h) on the promoter activity for EAAT3 in resistant HCT116 cells. Data are mean ± SD ($n = 3$). **$P < 0.01$ *versus* the control group. (H) Relative abundances of GSH, GSSG, and the GSH/GSSG ratio in mock-treated cells or cells transfected with siRNAs targeting STAT3 (siSTAT#1 or siSTAT#2). Data are mean ± SD ($n = 3$). *$P < 0.05$, **$P < 0.01$, ***$P < 0.001$ *versus* mock. (I) Effect of STAT3 knockdown or inhibition (2 μmol/L of BP-1-102) on the resistance to OXA (10 μmol/L, 72 h)

whether AKR1C1 increases glutathione levels by regulating EAAT1, EAAT2, and EAAT3. The resistant cell lines specifically expressed higher *EAAT3* mRNA and protein (Fig. 5A and B). Conversely, *EAAT3* knockdown with siRNA significantly down-regulated the GSH, GSSG, and the ratio of GSH/GSSG (Supporting Information Fig. S2 and Fig. 5C). To identify how AKR1C1 up-regulates EAAT3 in resistant cells, we proposed the signal transducer and activator of transcription 3 (STAT3) might be the central role since the pivotal role of AKR1C1 in the modulation of STAT3 phosphorylation[16]. Similar to the previous studies, the reciprocal endogenous co-immunoprecipitation experiments confirmed that ectopically expressed STAT3 was precipitated by AKR1C1 protein using the HA-tag (Fig. 5D), indicating a significant interaction between AKR1C1 and STAT3.

As a member of the STAT family, STAT3 typically resides in the cytoplasm in an inactive free form. Upon stimulation, it undergoes phosphorylation and translocation into the nucleus to transcribe targeted genes[17]. To elucidate this process, we performed cell fractionation and assessed STAT3 expression in nuclear and cytoplasmic sub-fractions. As depicted in Fig. 5E, increased STAT3 was observed in the nucleus, particularly in HCT116 cells stably expressing AKR1C1 with IL-6 stimulation. In contrast, depletion of AKR1C1 by siRNA in resistant cells down-regulated p-STAT3 (Tyr705) and EAAT3 expression (Fig. 5F). Dual-luciferase reporter analysis showed that the luciferase activity driven by EAAT3 promoters in resistant HCT116 cell lines was decreased by STAT3 inhibition with BP-1-102 (Fig. 5G, $P < 0.01$). Consistent with these results, the knockdown of STAT3 led to an inhibition of GSH, GSSG, and the ratio of GSH/GSSG in resistant HCT116 cell lines (Supporting Information Fig. S3 and Fig. 5H). When exposed to the STAT3 siRNAs or STAT3 inhibitor (2 μmol/L of BP-1-102), it could significantly reverse the resistance to OXA caused by overexpression of AKR1C1 in HCT116 cells (Fig. 5I, $P < 0.001$) and enhance the OXA sensitivity of AKR1C1 silence in the HCT116 resistant cells (Fig. 5J, $P < 0.001$). These results underscored the pivotal role of STAT3 in AKR1C1-mediated OXA resistance. Moreover, we investigated the expression levels of STAT3, p-STAT3, and EAAT3 in parental cells, AKR1C1-overexpressed cells, and OXA-R cells (Fig. 5K). Notably, OXA-R cells exhibited elevated p-STAT3 (Tyr705) levels and EAATs compared to parental control cells, suggesting a heightened activation status of STAT3 and EAAT3 in the OXA-resistant cells and the AKR1C1-overexpressed cells. Conversely, the knockdown of AKR1C1 in OXA-resistant cells led to a distinct decrease in p-STAT3 levels and EAAT3 (Fig. 5L).

In addition to EAAT3, the knockdown of AKR1C1 inhibited several downstream targets of STAT3. RNA-seq analyses demonstrated the distinct downregulation of cyclin D1, surviving, and MMP-2 in the OXA-resistant HCT116 cells (Fig. 5M). We next investigated how AKR1C1 interacts with STAT3. Based on the results of *in-silico* docking assays (Fig. 5N), the AKR1C1 mutations on its interface towards STAT3 impaired the interaction between AKR1C1 and STAT3 (Fig. 5O). Collectively, these findings reveal the role of AKR1C1 in promoting malignant proliferation and conferring OXA chemoresistance to colorectal cancer cells through the activation of the AKR1C1−STAT3−EAAT3 signaling pathway.

3.6. *Inhibition of AKR1C1 sensitizes colorectal cancer cells to OXA in vitro*

In our previous work, we have identified the natural product alantolactone (ALA) as one of the important inhibitors of AKR1C1[18]. As for OXA-resistant HCT116 cells, ALA also demonstrates a potent binding with AKR1C1 (Supporting Information Fig. S4). We next investigate the effect of ALA on OXA for the treatment of OXA-resistant colorectal cancer cells. According to the different concentration gradients and the corresponding inhibition index, the drug ZIP synergy scores were calculated using the online SiCoDEA (Single and Combined Drug Effect Analysis) app (Supporting Information Fig. S5). The maximum synergistic area was indicated by the white rectangle as shown in Fig. 6A. The findings demonstrated that 10 μmol/L represented the lowest concentration of ALA that fell within the region exhibiting the greatest degree of synergistic cytotoxicity. Consequently, the concentration of 10 μmol/L ALA was selected as the optimal concentration for combinatorial treatment regimens.

Subsequently, we monitored the cell growth curve of OXA-R cell lines treated with OXA (25 μmol/L), ALA (10 μmol/L), and the combination treatment. As illustrated in Fig. 6B, ALA exhibited a less inhibitory effect on cell growth, whereas the combination treatment significantly reduced cell growth compared to treatment with OXA alone ($P < 0.001$). To further verify the synergistic effect of ALA, the colony formation assay was conducted (Fig. 6C), demonstrating that the co-treatment of OXA with ALA was more effective in inhibiting colony numbers compared to treatment with OXA alone ($P < 0.01$). Furthermore, we investigated the effect of ALA on OXA-induced apoptosis by performing annexin V/PI staining and analyzing apoptosis markers through immunoblotting. The percentage of apoptotic cell population induced by OXA (25 μmol/L) was 10.7 ± 1.7%, which increased to 19.7 ± 3.1% when co-treated with ALA (10 μmol/L) (Fig. 6D and E). Similarly, the expression of cleaved-PARP and cleaved-caspase3 was enhanced under the combination treatment (Fig. 6F). These findings suggest that ALA sensitizes OXA-resistant HCT116 cells to OXA-induced growth inhibition and apoptosis.

Furthermore, we investigated whether ALA synergistically inhibited the expression levels of AKR1C1, p-STAT3, and EAAT3. Results in Fig. 6G demonstrate that ALA (10 μmol/L), particularly in combination with OXA, significantly reduced the expression of AKR1C1, p-STAT3 (Tyr705), and EAAT3 in OXA-R cells. As for the cellular redox homeostasis, the pharmacological inhibition of AKR1C1 with ALA abrogated the up-

caused by overexpression of AKR1C1 in HCT116 cells. ***$P < 0.001$. (J) Effect of STAT3 knockdown or inhibition (2 μmol/L of BP-1-102) on OXA sensitivity (10 μmol/L, 72 h) of AKR1C1 silence in the HCT116 resistant cells. ***$P < 0.001$. (K, L) Western blot analyses of AKR1C1, phosphor-STAT3 (Tyr705), total STAT3, EAAT3, and GAPDH in the indicated cell lines or experimental conditions. (M) Relative mRNA levels of AKR1C1, EAAT3, Cyclin D1, Survivin, and MMP-2 in mock-treated or AKR1C1 knockdown (siAKR#1, siAKR#2) HCT116-R cells determined by qRT-PCR. Data are mean ± SD ($n = 3$). *$P < 0.05$, **$P < 0.01$, ***$P < 0.001$. (N) Structural model of the AKR1C1−STAT3 interaction complex based on molecular docking simulations. Key residues involved in the interaction interface are labeled. (O) Co-immunoprecipitation of Flag-AKR1C1 and HA-STAT3 in HCT116-R cells under various AKR1C1 residue mutations. IP, immunoprecipitation; IB, immunoblotting.

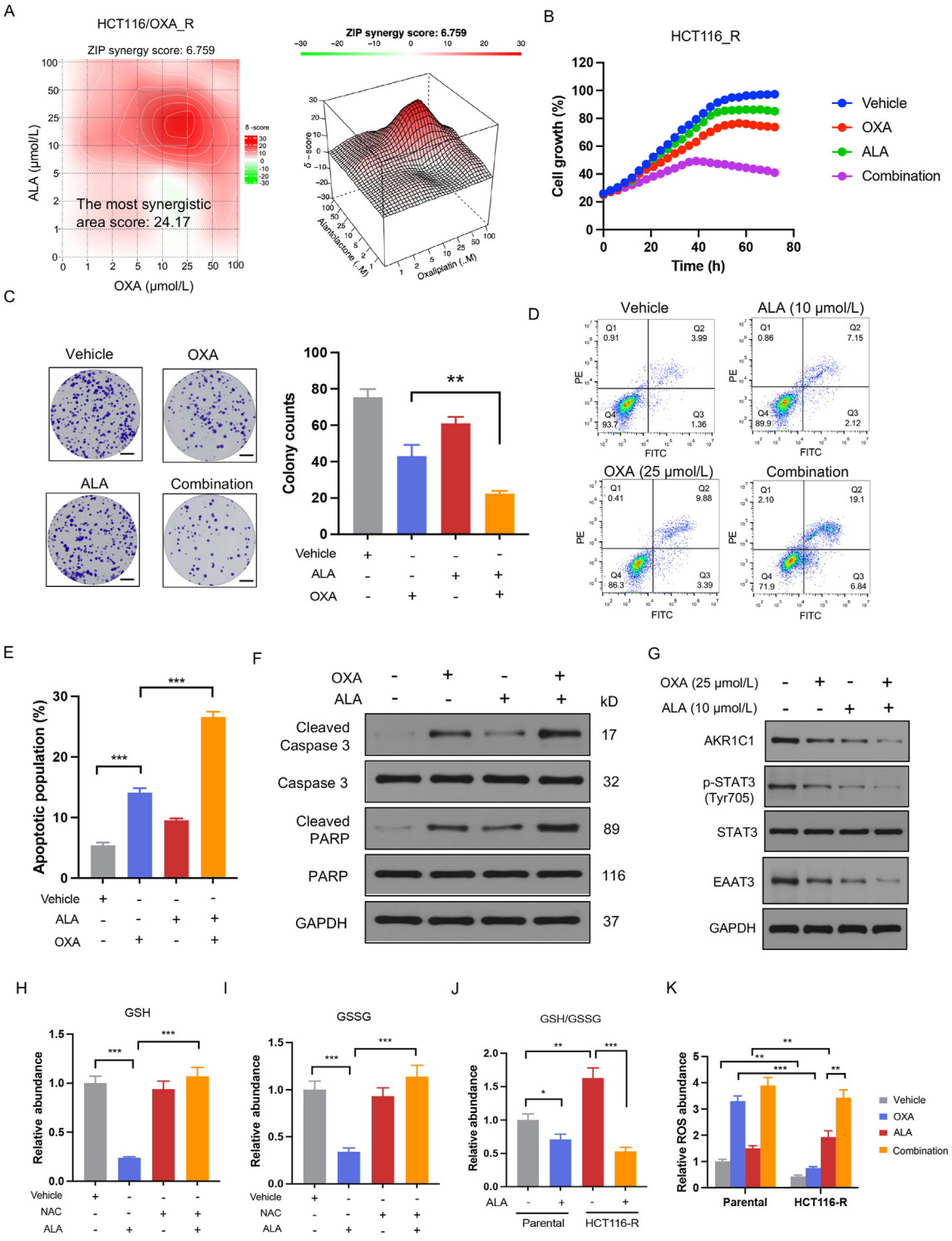

Figure 6 Inhibition of AKR1C1 sensitizes colorectal cancer cells to oxaliplatin (OXA) *in vitro*. (A) Heatmaps of drug combination responses. OXA and ALA act synergistically on HCT116 cells. OXA and alantolactone (ALA) at the indicated concentrations were used to treat cells for 48 h, and cell viability was assessed by CCK-8 assay. ZIP Synergy scores were calculated using Synergyfinder software. (B) Effect of ALA on OXA-resistant HCT116 cells by cell growth analysis. Cell growth was monitored and quantified using a live-cell analysis system (Axion BioSystems) every 4 h for 3 days. (C−F) Effect of ALA on OXA sensitivity in HCT116-resistant cells assayed by colony formation analysis (C, Scale bar = 5 mm), Annexin V-PI staining followed by flow cytometry analysis (D, E), and Western blot analysis for apoptosis markers (F). The cells were treated with 25 μmol/L OXA, or 10 μmol/L ALA alone, or a combination for 2 weeks for colony formation analysis and 48 h for flow cytometry analysis and Western blot analysis. (G) Effect of the combination of OXA with ALA on the expression of AKR1C1, p-STAT3 (Tyr705), and EAAT3. The cells were treated with 10 μmol/L ALA, or 25 μmol/L OXA alone, or a combination for 24 h. (H, I) The effect of the glutathione precursor *N*-acetylcysteine (NAC) on AKR1C1 inhibition induced suppression of GSH (H) and GSSG (I) in OXA-resistant HCT116 cells. Cells

regulated GSH, GSSG, and ratio of GSH/GSSG in OXA-resistant HCT116 cells, and this abrogation was restored by *N*-acetylcysteine supplement (Fig. 6H–J). The synergistic effects of ALA on the regulation of ROS levels in OXA-resistant HCT116 cells were also observed. Because of enhanced glutathione synthesis, the resistant cell lines accumulated less OXA-induced intracellular ROS compared with parental cell lines, and the reduced ROS level in OXA-resistant HCT116 cells was reversed by pharmacological inhibition of AKR1C1, evidenced by a significant increase of ROS when co-treated with ALA (Fig. 6K).

3.7. *Targeting of AKR1C1 sensitizes colorectal cancer cells to OXA in vivo*

To investigate the *in vivo* synergistic effect of the combination of the AKR1C1 inhibitor ALA with OXA, we established a xenograft model using BALB/c nude mice derived from resistant cells. Once the tumor volume reached 100 mm^3, the nude mice ($n = 6$) were randomly divided into four groups and received intravenous treatments of normal saline, OXA (20 mg/kg), ALA (15 mg/kg), or a combination of OXA and ALA. The drug administration was conducted on Days 1, 3, 5, 8, 10, 12, and 15, and the tumor volume was recorded until Day 19 (Fig. 7A). The results demonstrated that while the single agent ALA and OXA had minimal effects on tumor growth, the combination treatment exhibited a significantly greater inhibitory effect than either agent alone, resulting in a 57.8% tumor volume inhibition ($P < 0.05$, Fig. 7B and C) and without any body weight loss was found in both the individual agents and the combination treatment (Fig. 7D). Consistently, the average tumor weight was also reduced by the synergistic effect of the combination treatment (Fig. 7E).

We also evaluated the proliferation status of tumor tissues through immunohistochemical analysis. The combination of OXA and ALA significantly inhibited AKR1C1–STAT3–EAAT3 the signal pathway compared to treatment with OXA or ALA alone, as evidenced by the reduction in AKR1C1, p-STAT3 (Tyr705), and EAAT3 intensity based on the IHC staining (Fig. 7F). Moreover, the GSH content in the tumor samples was significantly reduced after the combination treatment (Fig. 7G), consistent with the findings from *in vitro* cell experiments. Therefore, the results from the animal model studies provided evidence of the synergistic effects of ALA on the sensitivity of OXA.

4. Discussion

OXA-based chemotherapy represents the first-line therapy for advanced colorectal cancer. However, the development of drug resistance following prolonged chemotherapies is virtually inevitable and consistently leads to treatment failure, posing a significant therapeutic challenge[19]. Despite extensive research, the precise mechanisms underlying chemoresistance to OXA remain incompletely understood. The present study unravels the crucial role of AKR1C1 in conferring resistance to OXA in CRC and highlights the therapeutic potential of targeting AKR1C1 to overcome OXA resistance. Our findings demonstrate that AKR1C1 interacts with and activates STAT3 to upregulate EAAT3, leading to the elevation of GSH levels in CRC cells. Moreover, the pharmacologic inhibition of AKR1C1 using alantolactone, a natural product inhibitor, could restore the sensitivity of resistant cell lines to OXA. A schematic representation of the proposed model illustrating the involvement of AKR1C1 in conferring OXA resistance is presented in Fig. 8.

AKR1C1 has been reported to drive the progression and metastasis of various cancers, including lung cancer, bladder cancer, and colorectal cancer[6,7,20]. Our study provides compelling evidence linking AKR1C1 expression to OXA sensitivity and poor prognosis in CRC patients. We observed a significant negative correlation between AKR1C1 expression levels and OXA sensitivity in a panel of NCI-60 CRC cell lines, suggesting that higher AKR1C1 expression confers resistance to OXA treatment. Increasing evidence suggests that AKR1C1 participates in several malignant biological processes, such as cell proliferation, invasion, and metastasis across different human cancer types[20-22]. Notably, AKR1C1 is implicated in chemotherapy resistance in gastric carcinoma, head and neck squamous cell carcinoma, lung cancer, colorectal cancer, and esophageal cancer[23,24]. Consistent with prior investigations, our study demonstrates that AKR1C1 expression not only promotes the malignant proliferation of colorectal cancer cells but also confers chemoresistance to OXA-induced cell apoptosis. These findings highlight the clinical relevance of AKR1C1 as a potential prognostic biomarker and therapeutic target in CRC.

Mechanistically, our study elucidates a novel regulatory axis involving AKR1C1, STAT3, and EAAT3, which contributes to OXA resistance through the modulation of cellular redox homeostasis. STAT3 is a key factor for cell growth, proliferation, and survival in different cancer cell lines, as well as chemotherapy resistance[25-27]. Previous studies have highlighted the ability of AKR1C1 to activate STAT3, thereby facilitating metastasis in non-small cell lung cancer and hepatocellular carcinoma[28]. Overexpression of AKR1C1 has been implicated in conferring cisplatin resistance in gastric carcinoma and head and neck squamous cell carcinoma through its interaction with the STAT3 signaling pathway[24]. Consistent with these findings, our study observed a close association between AKR1C1 and the activation of STAT3. Moreover, we demonstrated that AKR1C1 increases intracellular glutathione levels by up-regulating EAAT3 to confer resistance to OXA. EAAT3, a member of the EAAT family of high-affinity, sodium-dependent glutamate carriers, is involved in tumorigenesis by mediating cystine uptake and GSH biosynthesis[29,30]. Guo et al.[31] concluded that an EAAT3-dependent increase in glutamate influx confers lung cancer development. As one of the downstream target genes regulated by STAT3, we

were exposed to 10 μmol/L ALA for 6 h for AKR1C1 inhibition, 5 mmol/L NAC alone, or the indicated drug combinations for 6 h (mean ± SD, $n = 3$). ***$P < 0.001$. (J) The ratio of GSH/GSSG in resistant cells upon AKR1C1 pharmacological inhibition. Cells were treated with 10 μmol/L ALA for 6 h (mean ± SD, $n = 3$). *$P < 0.05$, **$P < 0.01$, ***$P < 0.001$. (K) The effect of AKR1C1 inhibition on OXA-induced intracellular ROS accumulation in resistant and parental HCT116 cells. The cells were treated with 10 μmol/L ALA, or 25 μmol/L OXA alone, or a combination for 6 h. ROS abundance in parental and resistant cells was determined by flow cytometry (mean ± SD, $n = 3$). **$P < 0.01$, ***$P < 0.001$.

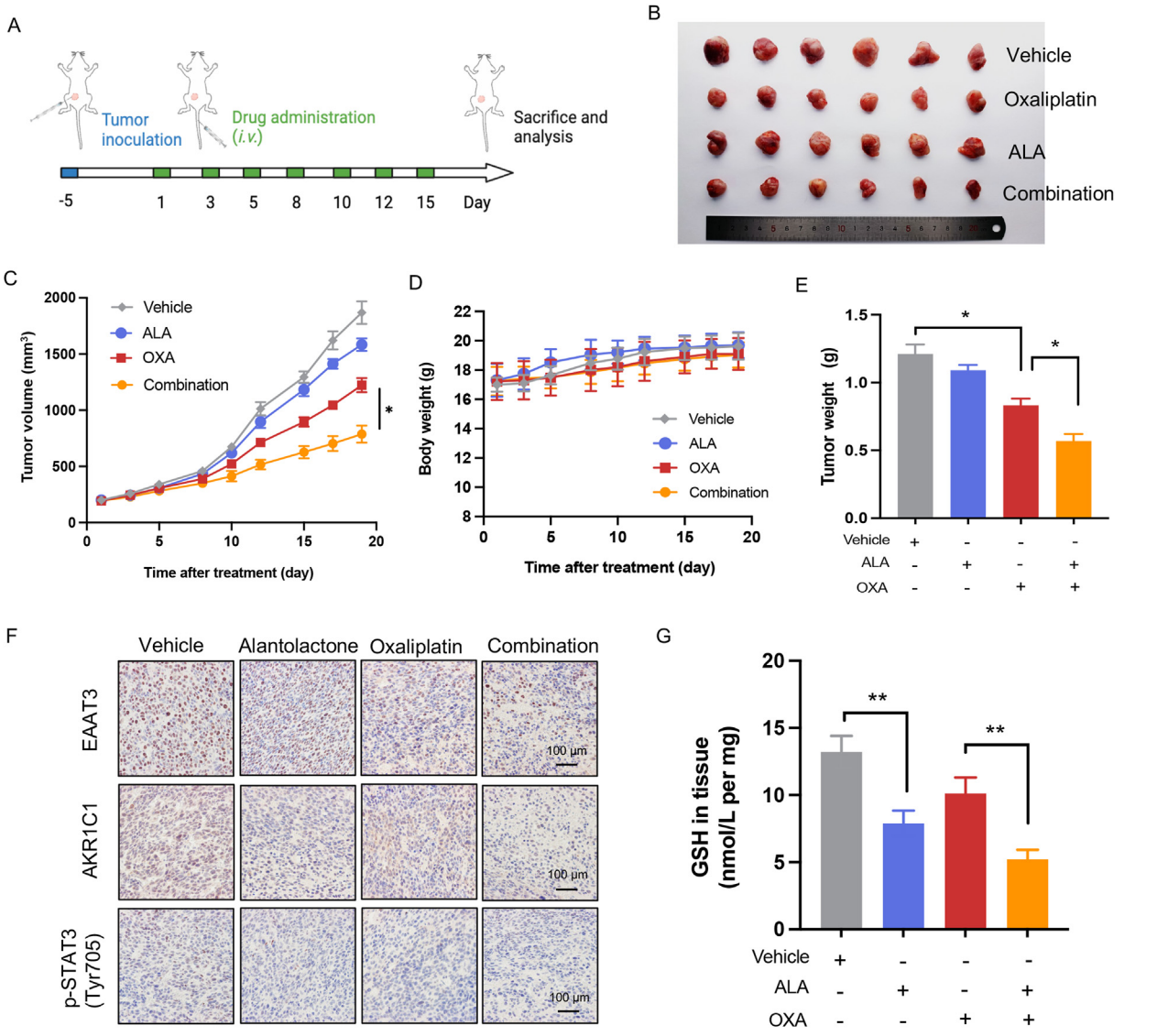

Figure 7 Targeting of AKR1C1 sensitizes colorectal cancer cells to oxaliplatin (OXA) *in vivo*. (A) Schedule of alantolactone (ALA) and/or OXA treatment on HCT116-R tumor-bearing mice. (B) Representative images of explanted tumors are presented. Scale bar, 1 cm. (C) Tumor volumes in the four groups were measured on the indicated days. Data are shown as mean ± SD ($n = 6$). *$P < 0.05$. (D) The body weights of mice in the four groups were recorded during the experiment. Data are shown as mean ± SD ($n = 6$). (E) The tumor weight changes in each arm after the experiment. Data are shown as mean ± SD ($n = 6$). *$P < 0.05$. (F) The effect of ALA on the AKR1C1−STAT3−EAAT3 signaling pathway was assessed by IHC staining in tumor tissues. The representative images are shown. Scale bar, 100 μm. (G) The measurement of GSH in tumor samples. Data are shown as mean ± SD ($n = 6$). **$P < 0.01$.

observed that EAAT3 knockdown abrogated the enhanced GSH/GSSG ratio in the OXA-resistant cells, underscoring the importance of this pathway in mediating AKR1C1-induced OXA resistance.

The maintenance of cellular redox homeostasis constitutes a prerequisite for cancer cell survival and proliferation[32]. In chemoresistant cells, reactive oxygen species are typically overproduced, necessitating concomitant upregulation of endogenous antioxidant systems to preserve redox balance[33]. GSH, a primary intracellular antioxidant, functions as the principal "defense shield" in drug-resistant cancer cells by preventing oxidative damage to vital cellular components induced by exogenous toxins and oxidants[34,35]. Elevated GSH levels have been observed in various platinum-resistant cancer cell lines[36,37]. Upon entry into the cytoplasm, platinum agents can be directly sequestered and inactivated through conjugation with GSH[38,39]. Moreover, this GSH conjugation facilitates the efflux of platinum drugs from cancer cells, thereby reducing their intracellular concentration[40]. Our study provides evidence that OXA-resistant cells exhibit elevated levels of GSH, regulated by AKR1C1, thereby suggesting the potential of targeting AKR1C1 to enhance sensitivity to OXA treatment.

Notably, the augmentation of STAT3 signaling and subsequent GSH level induced by AKR1C1 can be effectively reversed using a small molecule inhibitor, ALA, which specifically targets AKR1C1 and exerts a synergistic effect with OXA in inhibiting CRC cell growth both *in vitro* and *in vivo*. Moreover, the combination treatment significantly downregulated the AKR1C1−STAT3−EAAT3 axis, leading to decreased intracellular GSH/GSSG levels and increased ROS accumulation. These effects were further

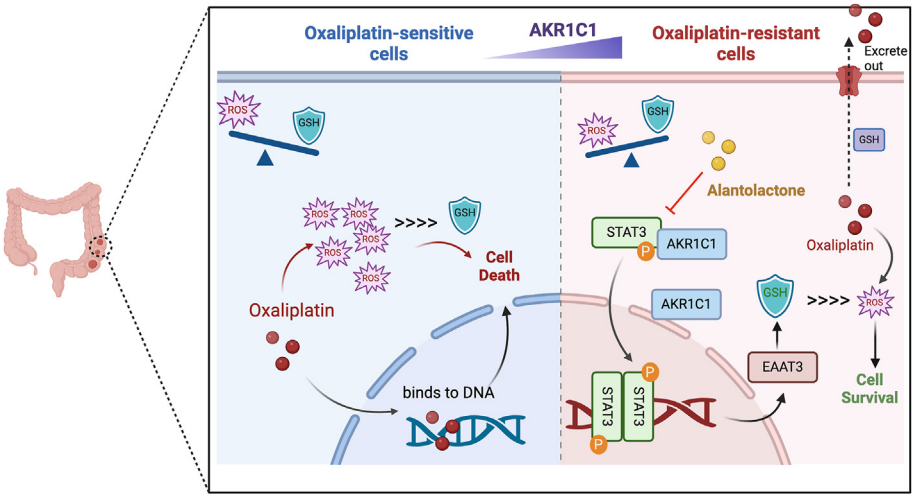

Figure 8 A schematic diagram illustrates the crucial role of AKR1C1 that drives the oxaliplatin (OXA) resistance in colorectal cancer cells. In the oxaliplatin-sensitive cells (left panel), OXA enters and causes DNA damage, leading to the production of reactive oxygen species (ROS). The ROS are initially counteracted by the antioxidant glutathione (GSH). However, excessive ROS overwhelms GSH, resulting in cell death *via* apoptotic pathways. In the OXA-resistant cells (right panel), the AKR1C1 is upregulated and interacts with STAT3 to facilitate its downstream target EAAT3 expression, leading to an elevated level of GSH. GSH levels are elevated, neutralizing ROS that caused OXA more effectively. Additionally, the excessive GSH would conjugate with OXA and promote the OXA to excrete out of cancer cells, which reduces the intracellular concentration of OXA in cancer cells. These coordinated mechanisms enable resistant cells to survive and proliferate despite OXA exposure. However, the pharmacological inhibition of AKR1C1 with alantolactone, a small-molecule inhibitor, could restore the sensitivity of resistant cell lines to OXA by blocking the interaction between AKR1C1 and STAT3.

corroborated *in vivo*, where the combination of ALA and OXA exhibited potent synergistic antitumor activity in a xenograft model, with significant inhibition of tumor growth and minimal toxicity. Importantly, the combination treatment effectively inhibited the AKR1C1−STAT3−EAAT3 signaling pathway and reduced GSH levels in tumor tissues, providing further mechanistic insights into the synergistic effects observed.

While our study provides compelling evidence for the role of AKR1C1 in OXA resistance, it is important to acknowledge potential limitations and considerations for future research. First, although we identified AKR1C1 as the most upregulated gene in OXA-resistant cells, other factors and signaling pathways may also contribute to the development of resistance. Further exploration of the complex interplay between different molecular mechanisms could provide a more comprehensive understanding of the chemoresistance landscape. Additionally, while we demonstrated the synergistic effects of ALA and OXA in preclinical models, it is essential to further evaluate this combination therapy in clinical settings. Pharmacokinetic and pharmacodynamic studies, as well as optimization of dosing regimens, would be necessary to promote the clinical transformation of these findings. Another consideration is the potential heterogeneity and plasticity of CRC tumors, which may influence the efficacy of targeting the AKR1C1 axis. It would be valuable to investigate the expression patterns and functional roles of AKR1C1 in different CRC subtypes and explore potential biomarkers or companion diagnostics to identify patients who are most likely to benefit from AKR1C1-targeted therapies.

5. Conclusions

Our study unveils a pivotal role for AKR1C1 in mediating OXA resistance in CRC and highlights the therapeutic potential of targeting the AKR1C1−STAT3−EAAT3 axis to overcome chemoresistance. The synergistic effects observed with the AKR1C1 inhibitor ALA and OXA provide a promising combinatorial strategy for enhancing the therapeutic efficacy of OXA in CRC patients. While further research is warranted to address potential limitations and translational challenges, our findings contribute to a deeper understanding of the biochemical pathways involved in chemoresistance in colorectal cancer and open avenues for innovative treatments that could significantly impact patient management and survival.

Acknowledgments

This work was supported by the National Natural Science Foundation of China (Grant Nos. 82204758 and 82073402).

Author contributions

Zhiwen Fu: Writing − review & editing, Writing − original draft, Funding acquisition, Data curation, Conceptualization. Tingting Wu: Software, Methodology, Investigation. Chen Gao: Validation, Software, Methodology. Lulu Wang: Software, Methodology. Yu Zhang: Writing − review & editing. Chen Shi: Writing − review & editing, Supervision, Funding acquisition, Conceptualization.

Conflicts of interest

The authors declare no conflicts of interest.

Appendix A. Supporting information

Supporting information to this article can be found online at https://doi.org/10.1016/j.apsb.2024.08.031.

References

1. Sung H, Ferlay J, Siegel RL, Laversanne M, Soerjomataram I, Jemal A, et al. Global cancer statistics 2020: GLOBOCAN estimates of incidence and mortality worldwide for 36 cancers in 185 countries. *CA Cancer J Clin* 2021;**71**:209−49.
2. Sharif S, O'Connell MJ, Yothers G, Lopa S, Wolmark N. FOLFOX and FLOX regimens for the adjuvant treatment of resected stage II and III colon cancer. *Cancer Invest* 2008;**26**:956−63.
3. Taieb J, Gallois C. Adjuvant chemotherapy for stage III colon cancer. *Cancers* 2020;**12**:2679.
4. Mauri G, Gori V, Bonazzina E, Amatu A, Tosi F, Bencardino K, et al. Oxaliplatin retreatment in metastatic colorectal cancer: systematic review and future research opportunities. *Cancer Treat Rev* 2020;**91**: 102112.
5. Zhang Y, Li C, Liu X, Wang Y, Zhao R, Yang Y, et al. circHIPK3 promotes oxaliplatin-resistance in colorectal cancer through autophagy by sponging miR-637. *EBioMedicine* 2019;**48**:277−88.
6. Zeng CM, Chang LL, Ying MD, Cao J, He QJ, Zhu H, et al. Aldo−keto reductase AKR1C1−AKR1C4: functions, regulation, and intervention for anti-cancer therapy. *Front Pharmacol* 2017;**8**:119.
7. Matsumoto R, Tsuda M, Yoshida K, Tanino M, Kimura T, Nishihara H, et al. Aldo−keto reductase 1C1 induced by interleukin-1β mediates the invasive potential and drug resistance of metastatic bladder cancer cells. *Sci Rep* 2016;**6**:34625.
8. Zhou C, Shen G, Yang F, Duan J, Wu Z, Yang M, et al. Loss of AKR1C1 is a good prognostic factor in advanced NPC cases and increases chemosensitivity to cisplatin in NPC cells. *J Cel Mol Med* 2020;**24**:6438−47.
9. Huang F, Zheng Y, Li X, Luo H, Luo L. Ferroptosis-related gene AKR1C1 predicts the prognosis of non-small cell lung cancer. *Cancer Cel Int* 2021;**21**:1−16.
10. Matsunaga T, Suzuki A, Kezuka C, Okumura N, Iguchi K, Inoue I, et al. Aldo−keto reductase 1B10 promotes development of cisplatin resistance in gastrointestinal cancer cells through down-regulating peroxisome proliferator-activated receptor-γ-dependent mechanism. *Chem Biol Interact* 2016;**256**:142−53.
11. Chang Q, Petrash JM. Disruption of aldo−keto reductase genes leads to elevated markers of oxidative stress and inositol auxotrophy in Saccharomyces cerevisiae. *Biochim Biophys Acta Mol Cel Res* 2008; **1783**:237−45.
12. Jin Y, Penning TM. Aldo−keto reductases and bioactivation/detoxication. *Annu Rev Pharmacol Toxicol* 2007;**47**:263−92.
13. Lai Y, Chu X, Di L, Gao W, Guo Y, Liu X, et al. Recent advances in the translation of drug metabolism and pharmacokinetics science for drug discovery and development. *Acta Pharm Sin B* 2022;**12**: 2751−77.
14. Penning TM. Aldo−keto reductase regulation by the Nrf2 system: implications for stress response, chemotherapy drug resistance, and carcinogenesis. *Chem Res Toxicol* 2017;**30**:162−76.
15. Ghoneum A, Abdulfattah AY, Warren BO, Shu J, Said N. Redox homeostasis and metabolism in cancer: a complex mechanism and potential targeted therapeutics. *Int J Mol Sci* 2020;**21**:3100.
16. Gargalionis AN, Papavassiliou KA, Papavassiliou AG. Targeting STAT3 signaling pathway in colorectal cancer. *Biomedicines* 2021;**9**: 1016.
17. Mohassab AM, Hassan HA, Abdelhamid D, Abdel-Aziz M. STAT3 transcription factor as target for anti-cancer therapy. *Pharmacol Rep* 2020;**72**:1101−24.
18. Fu Z, Li S, Liu J, Zhang C, Jian C, Wang L, et al. Natural product alantolactone targeting AKR1C1 suppresses cell proliferation and metastasis in non-small-cell lung cancer. *Front Pharmacol* 2022;**13**: 847906.
19. Okon IS, Zou MH. Mitochondrial ROS and cancer drug resistance: implications for therapy. *Pharmacol Res* 2015;**100**:170−4.
20. Zhu H, Hu Y, Zeng C, Chang L, Ge F, Wang W, et al. The SIRT2-mediated deacetylation of AKR1C1 is required for suppressing its pro-metastasis function in non-small cell lung cancer. *Theranostics* 2020;**10**:2188.
21. Wei X, Wei Z, Li Y, Tan Z, Lin C. AKR1C1 contributes to cervical cancer progression *via* regulating TWIST1 expression. *Biochem Genet* 2021;**59**:516−30.
22. Qiao L, Shi C, Gao J, Liu Y, Zheng Q. AKR1C1 overexpression attenuates the inhibitory effect of glycyrrhizic acid on gastric cancer cell proliferation and migration. *Trop J Pharm Res* 2022;**21**:707−14.
23. Phoo NLL, Dejkriengkraikul P, Khaw-On P, Yodkeeree S. Transcriptomic profiling reveals AKR1C1 and AKR1C3 mediate cisplatin resistance in signet ring cell gastric carcinoma *via* autophagic cell death. *Int J Mol Sci* 2021;**22**:12512.
24. Chang WM, Chang YC, Yang YC, Lin SK, Chang PMH, Hsiao M. AKR1C1 controls cisplatin-resistance in head and neck squamous cell carcinoma through cross-talk with the STAT1/3 signaling pathway. *J Exp Clin Cancer Res* 2019;**38**:245.
25. Han D, Yu T, Dong N, Wang B, Sun F, Jiang D. Napabucasin, a novel STAT3 inhibitor suppresses proliferation, invasion and stemness of glioblastoma cells. *J Exp Clin Cancer Res* 2019;**38**:289.
26. Yang PL, Liu LX, Li EM, Xu LY. Stat3, the challenge for chemotherapeutic and radiotherapeutic efficacy. *Cancers* 2020;**12**:2459.
27. Zhao D, Zhang J, Zhang L, Wu Q, Wang Y, Zhang W, et al. PAFR/-Stat3 axis maintains the symbiotic ecosystem between tumor and stroma to facilitate tumor malignancy. *Acta Pharm Sin B* 2023;**13**: 694−708.
28. Hong Z, Chang LL, Fang-Jie Y, Yan H, Chen-Ming Z, Tian-Yi Z, et al. AKR1C1 activates STAT3 to promote the metastasis of non-small cell lung cancer. *Theranostics* 2018;**8**:676.
29. Lewerenz J, Hewett SJ, Huang Y, Lambros M, Gout PW, Kalivas PW, et al. The cystine/glutamate antiporter system Xc^- in health and disease: from molecular mechanisms to novel therapeutic opportunities. *Antioxid Redox Signal* 2013;**18**:522−55.
30. Liu X, Zhang Y, Zhuang L, Olszewski K, Gan B. NADPH debt drives redox bankruptcy: SLC7A11/xCT-mediated cystine uptake as a double-edged sword in cellular redox regulation. *Genes Dis* 2021;**8**: 731−45.
31. Guo W, Li K, Sun B, Xu D, Tong L, Yin H, et al. Dysregulated glutamate transporter SLC1A1 propels cystine uptake *via* Xc^- for glutathione synthesis in lung cancer. *Cancer Res* 2021;**81**:552−66.
32. Li Y, Zhang X, Wang Z, Li B, Zhu H. Modulation of redox homeostasis: a strategy to overcome cancer drug resistance. *Front Pharmacol* 2023;**14**:1156538.
33. Cui Q, Wang JQ, Assaraf YG, Ren L, Gupta P, Wei L, et al. Modulating ROS to overcome multidrug resistance in cancer. *Drug Resist Updat* 2018;**41**:1−25.
34. Liu J, Yuan Y, Cheng Y, Fu D, Chen Z, Wang Y, et al. Copper-based metal−organic framework overcomes cancer chemoresistance through systemically disrupting dynamically balanced cellular redox homeostasis. *J Am Chem Soc* 2022;**144**:4799−809.
35. Niu B, Zhou Y, Liao K, Wen T, Lao S, Quan G, et al. "Pincer movement": reversing cisplatin resistance based on simultaneous glutathione depletion and glutathione *S*-transferases inhibition by redox-responsive degradable organosilica hybrid nanoparticles. *Acta Pharm Sin B* 2022;**12**:2074−88.
36. Giaccone G. Clinical perspectives on platinum resistance. *Drugs* 2000; **59**:9−17.
37. Zhang L, Ye B, Chen Z, Chen ZS. Progress in the studies on the molecular mechanisms associated with multidrug resistance in cancers. *Acta Pharm Sin B* 2023;**13**:982−97.
38. Fronik P, Gutmann M, Vician P, Stojanovic M, Kastner A, Heffeter P, et al. A platinum (IV) prodrug strategy to overcome glutathione-based oxaliplatin resistance. *Commun Chem* 2022;**5**:46.
39. Criscuolo D, Avolio R, Parri M, Romano S, Chiarugi P, Matassa DS, et al. Decreased levels of GSH are associated with platinum resistance in high-grade serous ovarian cancer. *Antioxidants* 2022;**11**:1544.
40. Pearson SA, Cowan J. Glutathione-coordinated metal complexes as substrates for cellular transporters. *Metallomics* 2021;**13**:mfab015.